Control of a Hybrid Helicopter with Wings

Wagter, Christophe De; Smeur, Ewoud

Control of a hybrid helicopter with wings

C. De Wagter[*] and E.J.J. Smeur[†]

Delft University of Technology, Kluyverweg 1, 2629HS Delft, the Netherlands

ABSTRACT

This work investigates the design parameters and consequences in the control of a helicopter rotor combined with a pair of fixed wings. This hybrid vehicle has a light and aerodynamically efficient rotor that can achieve large pitch angles to allow forward flight. Because of the light stiff rotor and heavy wings, the hybrid vehicle exhibits couplings between the roll and pitch axes during hover flight. The rotor-wing interaction depends on a lot of parameters. In this paper, we utilize a simplified theoretic model and simulations in order to gain insight in the effect of these parameters on the vehicle dynamics. Finally, a controller is designed that compensates undesired coupling between pitch and roll.

1   INTRODUCTION

Rotorcraft dynamics have been well studied for many years[1, 2, 3, 4] with work ranging from rotorcraft modeling [5, 6], simulation [7], over matching measurement data with models [8], to the blade optimization in function of vibrations [9].

The design of controllers for conventional helicopters is well understood [10][11].

For less conventional designs like hinge-less low inertia rotors or high inertia fuselages, the design choices and control problems are more complex. Some studies into the fuselage-rotor interaction and fuselage ground interaction have identified resonance problems [12].

On the scale of small unmanned helicopters, models were used to identify which parameters affect the performance [13] and to reduce vibrations or noise [14]. Recent work presents a comprehensive non-linear model of a miniature unmanned helicopter [6].

1.1   Heli-Wing Hybrid

The approach of using a model to identify parameters important for the performance can also be applied to a vehicle such as a heli-wing hybrid. But when designing hybrid vehicles different parameters are important.

The subject of this paper is the design and control of a conventional cyclic and collective pitch controlled rotor on top of a fixed wing shaped heavy fuselage. Figure 1 shows the vehicle in semi transitioned attitude. The rotor allows the

---

*Email address: c.dewagter@tudelft.nl
†Email address: e.j.j.smeur@tudelft.nl

vehicle to hover while the wings and rotor design enable efficient fast forward flight.

Figure 1: Novel hybrid Unmanned Air Vehicle featuring a cyclic controlled rotor with wing.

The rotor blade design in the case of this vehicle is a compromise between efficient hover and efficient forward flight. This means the rotor is significantly different from rotors seen in conventional helicopters. It is relatively small, light, stiff and it has a high lift coefficient. During forward flight the *rpm* is reduced and pitch angle increased to generate propulsion efficiently. The wings which act as fuselage are large and systems are distributed over the entire wing, giving it a large moment of inertia.

These properties significantly affect the way the conventional helicopter rotor behaves during hover. On the other hand, during forward flight, the propulsion gyroscopic effect is much larger than usual, which also has an influence on the vehicle's dynamics.

In order to find an acceptable compromise between the dynamics in hover and forward flight, a mathematical model is created in Section 2. Design parameters are varied in Section 3. Section 4 investigates the interaction between rotor and fuselage and in Section 5 the model is used to gain insight in the flight test results of hovering flight.
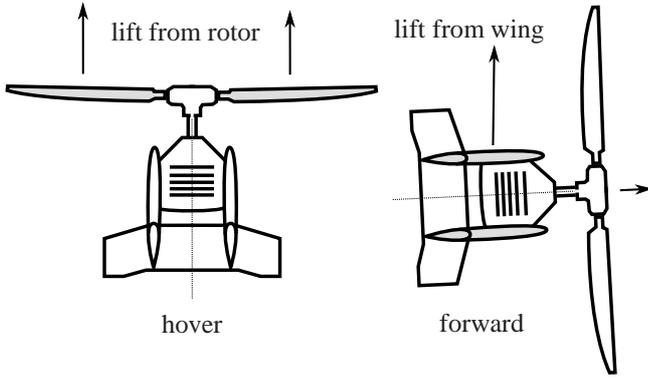
Figure 2: Hover and forward flight.

2 ROTOR MODEL

To explore the design options and their consequences, a helicopter model is derived mathematically. Figure 3 illustrates the basic rotor model [1]. The flapping angle β is measured around the spring hinge K. The rotor radius is R and it is spinning with a rate ω. The inputs are deflections of the swash-plate around the body X axis δ_x and Y axis δ_y. A positive input δ_x increases the pitch of the blade as it passes over the Y axis.
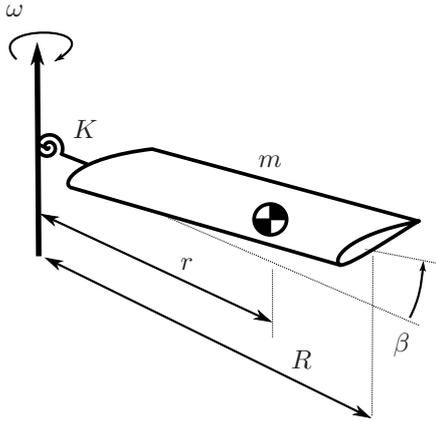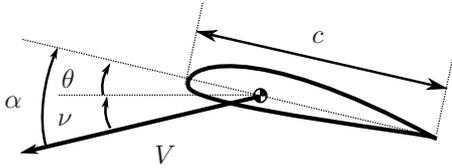

Figure 3: Simplified Rigid Rotor Model.

Figure 4: Angle of attack on a rotor section.

The forces acting on a blade element and the corresponding angles are illustrated in Figure 4. The model neglects the lagging angle of the rotor blade. The velocity V_x of the blade

element then becomes ωr while the vertical speed of the blade element V_y is a function of the flapping rate $\dot{\beta} r$. The path angle ν is the arc tangent of V_x and V_y while θ is the feathering angle of the blade and is set with collective and cyclic pitch commands.

$$\bar{V} = \begin{pmatrix} V_x \\ V_y \end{pmatrix} = \begin{pmatrix} \omega r \\ \dot{\beta} r \end{pmatrix} \tag{1}$$

Since we are mainly interested in the lateral control properties, we will neglect collective pitch, meaning that there will be no induced velocity v_i and the angle of attack of a blade element is $\alpha = \theta + \nu$, and for small angles $\nu = \dot{\beta}/\omega$. The lift on a blade element becomes:

$$\delta L = \frac{\rho}{2}(\omega r)^2 c_{l_\alpha} \cdot c \delta r \tag{2}$$

in which c_{l_α} is the lift coefficient and ρ the air density. The *Lock Number* $\gamma = \rho c_{l_\alpha} c R^4 / I$ is substituted with I being the inertia of the rotor [1]. The radius r is made non-dimensionless as $x = r/R$ which yields:

$$\delta L = \gamma \frac{\omega^2 I}{R} \left(\theta - \frac{\dot{\beta}}{\omega} \right) \cdot \frac{1}{2} x^2 \cdot \delta x \tag{3}$$

The centrifugal force $\delta m \cdot r \cos(\beta) \cdot \omega^2$ and the aerodynamic force δL on a blade element together with the mass δm of the blade element yield the following moment equation at the hinge:

$$\int \delta L \cdot r - \int \delta m \cdot \omega^2 \cdot r \cos(\beta) \cdot r \sin(\beta) = \int r \cdot \delta m \tag{4}$$

δL is expressed in function of δr in Equation 3. δm can be expressed in function of a length unit δr using the rotor density ρ_{blade} and it's cross section $S_{cross\_section}$.

The hinge spring moment is given as $K \cdot \beta$. When linearizing Equation 4, filling the lift force from Equation 3 and integrating over a uniform rotor, the differential equation [1] for flapping around a fixed hinge is obtained:

$$\ddot{\beta} + \frac{\gamma}{8}\omega\dot{\beta} + (\omega^2 + \frac{K}{I})\beta = \frac{\gamma}{8}\omega^2(\theta) \tag{5}$$

Equation 5 relates the inertia of the rotor, the aerodynamic damping, the centrifugal and spring forces to the excitation. In simulation the rotor is defined as a finite number of sections and integral in Equation 4 is replaced by a summation over all segments.

The excitation using feathering angle θ is periodic and a function of the control inputs δ_x and δ_y

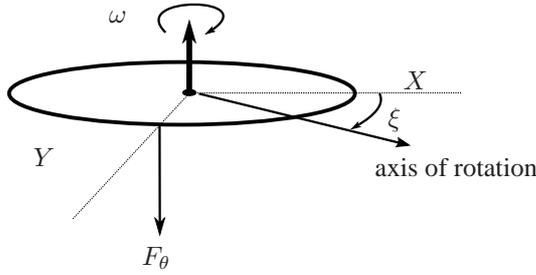$$\theta = \delta_y \sin(\omega t) + \delta_x \cos(\omega t) \tag{6}$$

Figure 5: Applied force F_θ on a spinning rotor and corresponding axis of rotation at angle ξ. For non spinning bodies ξ is zero as a moment in the X axis will produce a rotation in the X axis. For pure gyroscopes ξ is 90 degrees.

3   DESIGN VARIATION

The derived model is analyzed in simulation. To gain insight into the design choices, several variables in the model that can be tuned in real life are varied over a range.

3.1   Hinged Rotor

Figure 6 shows the results for a rotor with $K = 0$. Parameters for the model can be found in Section Appendix A:. A deflection δ_y of 4 degrees is applied. After a few rotations[1], the rotor plane is tilted.

The deflection β has a phase lag of 90 degrees with the perturbation θ as is expected in gyroscopes. ξ (See Figure ref-figure:Advance) is equal to 90 degrees. The cyclic deflection in pitch decreases the feathering angle θ whenever the rotor blade is at the right position of the ω clockwise spinning rotor, to yield a rotor-plane inclination backward.
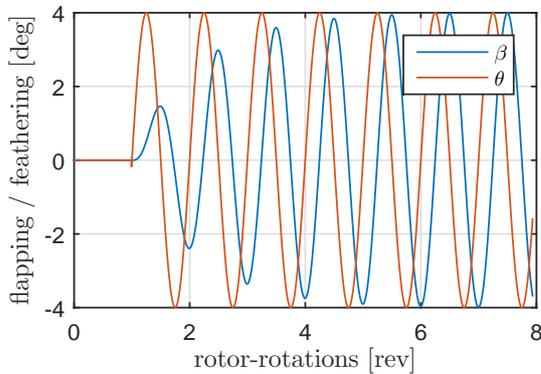

Figure 6: Blade dynamics based on cyclic deflection with zero spring stiffness K.

3.2   Stiff Rotor

When the stiffness of the spring K is increased, the dynamics of the rotor are significantly affected. Not only is

---

[1]The number of rotations depends on the *Lock Number* γ or in other words the damping to weight ratio.

the deflection β reduced, but also the direction flapping — in other words the rotor plane rotation — is affected.

Figure 7 shows the results for a rotor system with a stiff spring (high K). In this case the angle ξ, or in other words the phase difference between θ and β, is reduced from 90 degrees to below 30 degrees for a spring K which reduces the flapping angle β roughly by half.
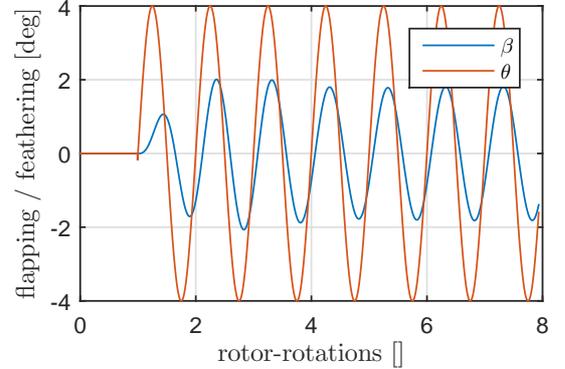

Figure 7: Blade dynamics based on cyclic deflection with significant spring stiffness K.

3.3   Design Parameters

From Equation 5 it can be found that the dynamics of the rotor are affected by its rotation rate ω, *Lock Number* γ and spring stiffness with respect to rotor inertia K/I.

For a given amount of lift, the *Lock Number* γ can only be altered by changing the rotor weight and will influence the speed of the response. High values of K can even change the direction of the actuator.

4   ROTOR HEAD AND FUSELAGE

4.1   Rotor Head Model

Since the previous sections have shown the importance of the hinge spring, the model of the actual rotor is investigated further. Figure 8 shows a cross section of the helicopter rotor head used in the platform from Figure 1. It consists of an aluminum head block on a main rotor shaft. The shaft holding both blades is only connected to the hub via rubber o-rings. A close up can be seen in Figure 13.

Modeling the bending of all parts of the rotor is complex. The exact bending of the feathering shaft, the blade grips and the blade itself contain a large number of parameters. Modeling how the force is transferred from the rotor system to the main rotor shaft is much easier as it only involves the rubber o-ring stiffness K_{o-ring} and their location l_{o-ring} as illustrated in Figure 9. For one blade the moment from the rotor on the rotor shaft becomes:

$$M_{rotor-shaft} = \Delta z_{o-ring} \cdot K_{o-ring} \cdot l_{o-ring} \quad (7)$$
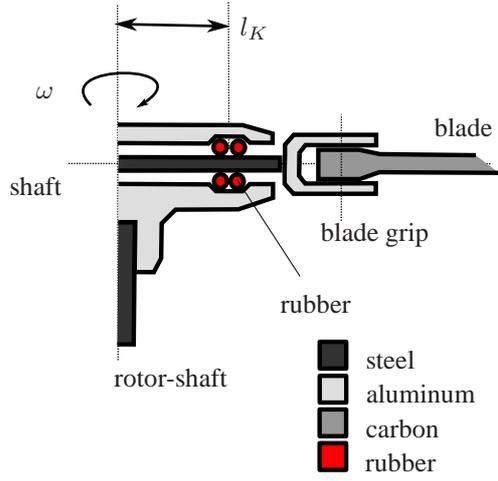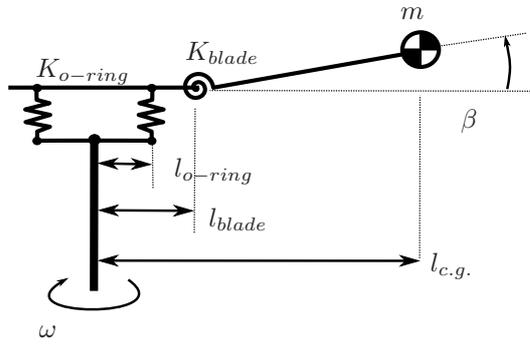
with

Figure 8: Actual Rotor Hub Simplified Schematics.

Figure 9: Simplified Rotor Hub.

$$\Delta z_{o-ring} = \frac{(M_{K_{blade}} + (\omega \cdot l_{c.g.})^2 m)}{l_{o-ring}} \qquad (8)$$

4.2 Constrained rotor-shaft motion

When the rotor shaft is rotated in pitch or roll to simulate a fuselage change in attitude, the rotor plane is following the fuselage motion. Figure 10 depicts the simulation results of a 10 degree pitch up of the fuselage and main rotor shaft in the case of a pure hinged rotor with $K = 0$ and in the case of a bending rotor with K non-zero.

In the case of a fully hinged rotor, the rotor disc still tracks the motion of the rotor-shaft, as the feathering angle of the blade remains parallel to the rotor shaft through the swash-plate dynamics. When neglecting the blade grip push-rods and swash-plate forces, the moment from rotor to rotor shaft is zero.

On the other hand, whenever a moment can be transferred from the rotor to the rotor-shaft, it can be seen that the relative blade flapping angle β_{shaft} creates moments M_x and M_y with a frequency of 2ω, or two times the rotor frequency.
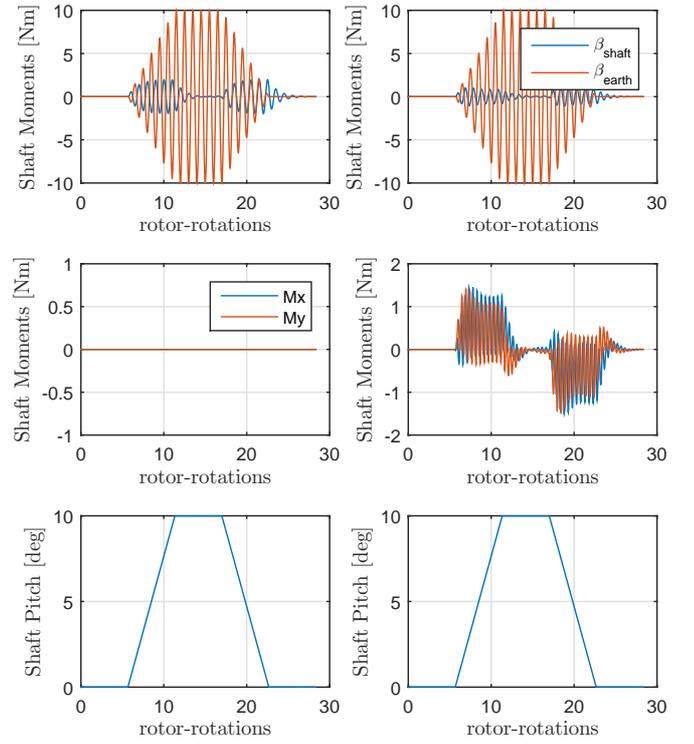

Figure 10: Rotor dynamics in function of fuselage imposed motion. Left $K = 0$, right $K \neq 0$.

It is interesting to note that a pure imposed pitch motion will generate moments in both M_x and M_y directions. The fuselage applies a moment to the rotor to make it pitch up, but the gyroscopic reaction of the rotor on that pitching motion is a rolling motion. This yields a roll moment from the rotor on the fuselage in return.

This is of particular importance in the case of a partially constrained fuselage. For instance, upon landing of the vehicle from Figure 1 with a roll angle, one tip will touch the ground first, yielding a constrained roll rate imposed on the rotor. As shown in Figure 10, this results in significant pitch moments imposed back from the rotor on the fuselage, which can cause undesired pitch motions caused by imposed roll motions.

Similarly, in forward flight, a pitching moment from the fixed wing and its elevons will cause an undesired yawing moment from the rotor back on the fuselage.

4.3 Free fuselage dynamics

To simulate the free fuselage dynamics, the fuselage is modeled as four point loads of a quarter of the total mass. The fuselage is symmetric around the X and Y axis but the dimensions are not equal.

The distance from the real center of gravity to each point load in the x direction is l_x and in the y direction l_y.
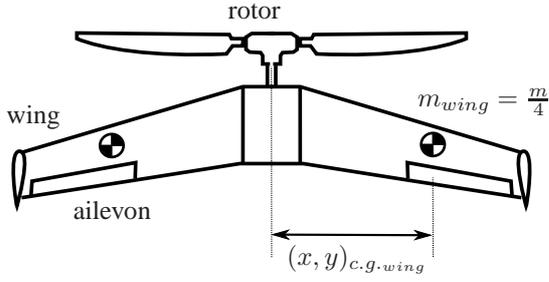
Figure 11: Body Model.

$$I_{xx} = \frac{m}{4} \cdot x_{c.g.wing} \qquad (9)$$

$$I_{yy} = \frac{m}{4} \cdot y_{c.g.wing} \qquad (10)$$

Assuming no aerodynamic forces on the wing during hover, no yaw rate and small angles, the fuselage rates are obtained through integration of the rotor shaft moments.

$$p_{fuselage} = \int_0^t \frac{M_x}{I_{xx}} dt \qquad (11)$$

$$q_{fuselage} = \int_0^t \frac{M_y}{I_{yy}} dt \qquad (12)$$

5 CONTROL CONSIDERATIONS

The derived models were applied to the rotor design of the hybrid rotor-wing vehicle depicted in Figure 1. Its light carbon rotor, mounted on a stiff conventional rotor head with high lift coefficient rotor blade airfoils — parameters given in Section Appendix A: — is not behaving like a conventional helicopter anymore.

To validate the model, real flight tests were performed. A governor was programmed to yield a constant rpm, to remove extra variables from the problem. Figure 14 shows the rpm is kept constant as soon as the vehicle takes off. The flight controller used is the paparazzi autopilot project [15, 16].

The vehicle can be flown with a simple proportional controller that controls the vehicle's angular rates. The output of this controller are cyclic commands, which are mapped to the three servos that control the swash-plate. The feedback was initially done with a 90 degree offset, such that roll feedback was applied to δ_x and pitch feedback to δ_y. δ_x produces a moment in the pitch axis and δ_y produces a moment in the roll axis. Due to gyroscopic precession this then produces an angular rate in the correct axis. This method of control is very common for helicopters [1].

For the vehicle in question, this controller did not provide control without couplings. Inputs of the pilot resulted in rates in a different axis than intended and on top of that a transient 'wobble', where the vehicle oscillates in both pitch
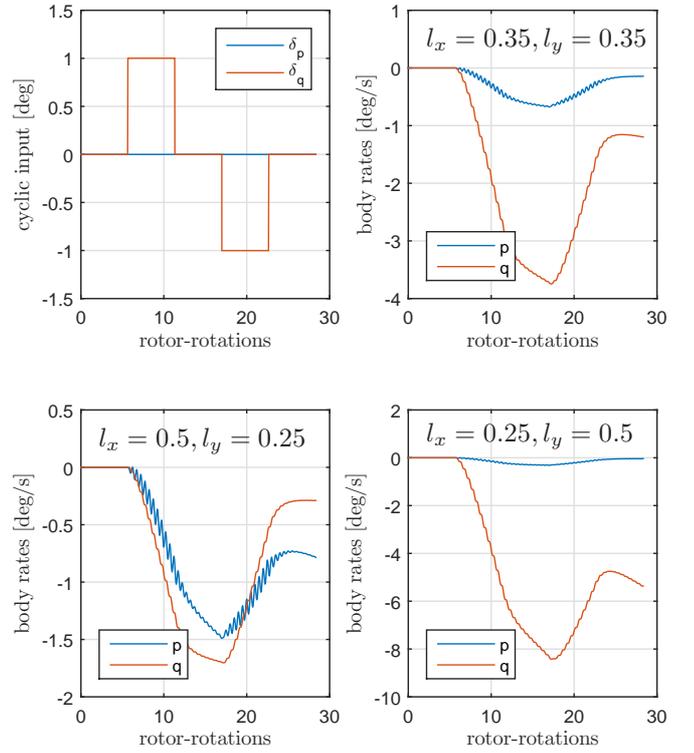

Figure 12: The influence of fuselage inertia on a free body. Three simulations of an identical rotor with identical non-zero stiffness and different inertia distribution of the fuselage.

and roll with a 90 degree phase difference. Using an onboard logging on an SD card, all turn rates and control deflections were logged. This data was used to model the angular acceleration in pitch and roll using the inputs δ_x and δ_y, the rates in roll and pitch and an offset $O = 1$. The model is shown in Equations 13 and 14, where f_p and f_q are linear functions of the parameters.

$$\dot{p} = f_p(O, \delta_x, \delta_y, p, q) \qquad (13)$$

$$\dot{q} = f_q(O, \delta_x, \delta_y, p, q) \qquad (14)$$

From the first data-set, it was discovered that the control mapping was incorrect, as δ_x and δ_y both caused a roll as well as a pitch acceleration. This was expected to cause some of the problems, which is why a second test flight was conducted using the correct control mapping.

Figure 15 shows the angular acceleration in roll and pitch along with the best fit of $f_p()$ and $f_q()$ for this second flight [17]. All signals were filtered with a second order filter with a cutoff frequency of 15 rad/s. The plot is taken during a 20 degree step in roll. From the figure it can be seen that the model fit is very accurate for this part of the flight. However, it is also clear from the figure that the transient wobble was still present. This is attributed to the effect of the rate on
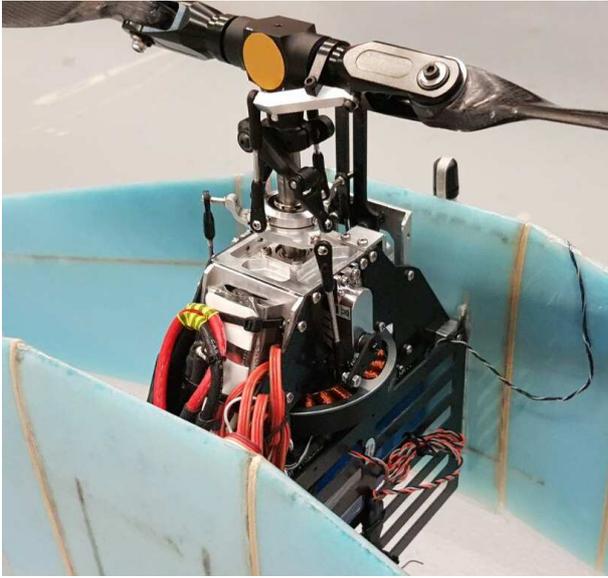
Figure 13: Close up of the rotor head of the hybrid winged helicopter vehicle. The swash-plate has 3 servos at 120 degrees from each other. Collective pitch has much greater reach than conventional helicopters and the blades have more twist to allow efficient forward flight.
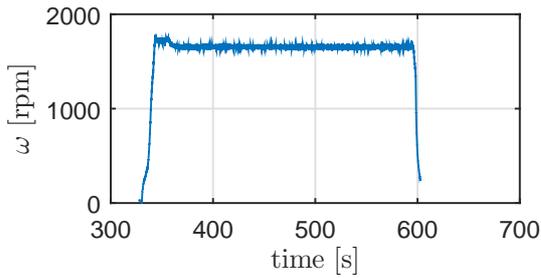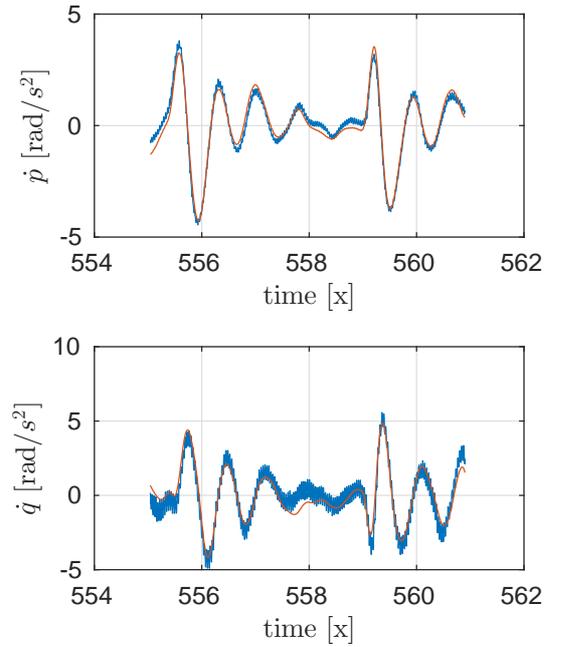

Figure 14: Test Flight RPM.

Figure 15: Fitting control inputs and body rates to body accelerations. In blue the filtered angular acceleration and in red the best model fit.

Coefficient	f_p	f_q
C_O	-2.4661	-2.8847
C_{δ_x}	0.0032	-0.0044
C_{δ_y}	0.0011	0.0073
C_p	-0.5703	7.4479
C_q	-3.4308	-3.4487

Table 1: Identified parameters.

angular acceleration in the other axis. The coefficients that were found using the data shown in Figure 15 are shown in Table 1.

Note the coefficients for C_p and C_q. They state that a roll rate causes a pitch acceleration and vice verse. This might well explain the observed wobble. Therefore, in order to remove the wobble, the angular acceleration due to the rates needs to be canceled by a control input. The linear controller is revised to:

$$\begin{bmatrix} \delta_x \\ \delta_y \end{bmatrix} = G^{-1} \begin{bmatrix} K_p p_{err} + q C_{q_{\dot{p}}} K_c \\ K_q q_{err} + p C_{p_{\dot{q}}} K_c \end{bmatrix} \quad (15)$$

Where p_err and q_err are the difference between the pilot command and the actual rates of the vehicle, and

$$G = \begin{bmatrix} C_{\delta_{x_{\dot{p}}}} & C_{\delta_{y_{\dot{p}}}} \\ C_{\delta_{x_{\dot{q}}}} & C_{\delta_{y_{\dot{q}}}} \end{bmatrix} \quad (16)$$

And K_c is a value between 0 and 1. K_c was introduced in order to gradually enable the compensation of angular acceleration due to rates. Test flights showed that a value of 0.5 gives better results than a value of 1. This may be caused by actuator dynamics, as a control moment can not be instantly generated when a rate is measured. More research is necessary to better explain why $K_c = 1$ still gives a wobble.

Figure 17 shows the measured angular rates of the vehicle during some pitch maneuvers in the first part of the flight and some roll maneuvers in the second part of the flight. The rates were filtered with a second order filter with a cutoff frequency of 25 rad/s. From this figure it can be seen that no wobble is present, and the motion in roll and pitch is uncoupled. Compare this to Figure 16, where $K_c = 0$ results in clear coupling between roll and pitch.
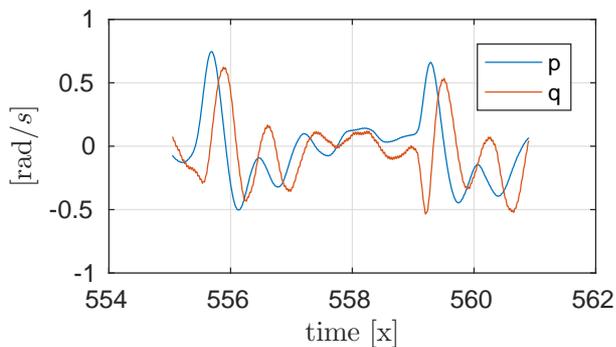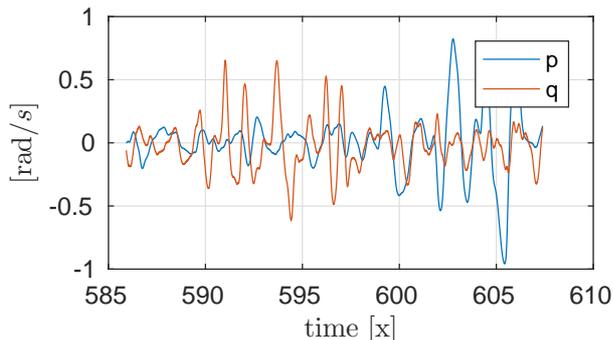
Figure 16: Flight with $K_c = 0$.

Figure 17: Flight with $K_c = 0.5$.

6 CONCLUSION

When designing hybrids between conventional cyclic controlled helicopters and fixed wings, it is crucial to understand the interactions between rotor and wing in order to optimize the design.

Lock Number and rotor hinge spring stiffness where shown to influence the speed and even direction of the control effectiveness.

Non-homogeneous inertia of the fuselage and fuselage-rotor interactions add non-symmetrical coupling between the pitch and roll axes. Compensation for gyroscopic effects was needed in the controller to remove this coupling.

ACKNOWLEDGMENTS

REFERENCES

[1] Anthony RS Bramwell, David Balmford, and George Done. *Bramwell's helicopter dynamics*. Butterworth-Heinemann, 2001.

[2] Raymond W Prouty. *Helicopter performance, stability, and control*. 1995.

[3] J Wagtendonk. Principles of helicopter flight by w. 1996.

[4] Wieslaw Zenon Stepniewski and CN Keys. *Rotary-wing aerodynamics*. Courier Corporation, 1979.

[5] Wayne Johnson. A comprehensive analytical model of rotorcraft aerodynamics and dynamics. part 1. analysis development. Technical report, DTIC Document, 1980.

[6] T. H. Lee G. Cai, B. M. Chen and K.-Y. Lum. Comprehensive nonlinear modeling of a miniature unmanned helicopter. *Journal of the American Helicopter Society*, 57(1):1–13, january 2012.

[7] Gareth D Padfield. *Helicopter flight dynamics*. John Wiley & Sons, 2008.

[8] Gloria K Yamauchi, Ruth M Heffernan, and Michel Gaubert. Correlation of sa349/2 helicopter flight test data with a comprehensive rotorcraft model. *Journal of the American Helicopter Society*, 33(2):31–42, 1988.

[9] David A Peters, Timothy Ko, Alfred Korn, and Mark P Rossow. Design of helicopter rotor blades for desired placement of natural frequencies. 1984.

[10] H Shim, Tak John Koo, Frank Hoffmann, and Shankar Sastry. A comprehensive study of control design for an autonomous helicopter. In *In: Proc. 37th IEEE Conf. on Decision and Control (CDC98*. Citeseer, 1998.

[11] Vladislav Gavrilets. Dynamic model for a miniature aerobatic helicopter. In *Handbook of Unmanned Aerial Vehicles*, pages 279–306. Springer, 2015.

[12] Robert A Ormiston. Rotor-fuselage dynamics of helicopter air and ground resonance. *Journal of the American Helicopter Society*, 36(2):3–20, 1991.

[13] FX Caradonna and Chee Tung. Experimental and analytical studies of a model helicopter rotor in hover. 1981.

[14] G Bernardini, E Piccione, A Anobile, J Serafini, and M Gennaretti. Optimal design and acoustic assessment of low-vibration rotor blades. *International Journal of Rotating Machinery*, 2016, 2016.

[15] Pascal Brisset, Antoine Drouin, Michel Gorraz, Pierre-Selim Huard, and Jeremy Tyler. The paparazzi solution. In *MAV 2006, 2nd US-European Competition and Workshop on Micro Air Vehicles*, pages pp–xxxx, 2006.

[16] Balazs Gati. Open source autopilot for academic research-the paparazzi system. In *American Control Conference (ACC), 2013*, pages 1478–1481. IEEE, 2013.

[17] Ewoud J. J. Smeur, Qiping P. Chu, and Guido C. H. E.
de Croon. Adaptive Incremental Nonlinear Dynamic
Inversion for Attitude Control of Micro Aerial Vehi-
cles. *Journal of Guidance, Control, and Dynamics*,
39(3):450–461, March 2016.

APPENDIX A: DATA

Parameters of the model are supplied below:

Variable	Value	Unit
R	51	cm
$r_{c.g.}$	30	cm
m	55	gram
c_{tip}	3.0	cm
c_{root}	5.7	cm
c_{l_α}	2π	cm
K	88	Nm/rad

Table 2: Blade parameters.

Variable	Value	Unit
$x_{c.g.wing}$	.8	m
$y_{c.g.wing}$	.12	m
m_{wing}	0.95	kg
m_{total}	3.9	kg

Table 3: Fuselage parameters.

Variable	Value	Unit
m_{weight}	730	gram
r_{weight}	41	cm
$r_{deflect}$	41	cm
$\Delta_{z_{tip}}$	17	mm

Table 4: Central Rotor Block Spring Mounts.

To asses the stiffness of the central rotor block rubbers,
a setup was created using a dummy weight to measure the
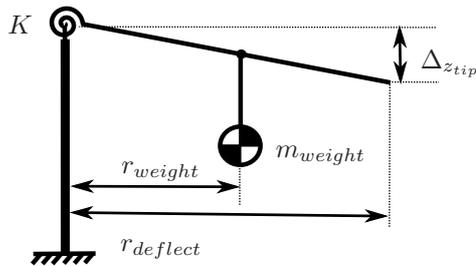increase in deflection as shown in Figure 18 with parameters
from Table 4.

Figure 18: Stiffness measuring.